INTERNATIONAL JOURNAL OF OPTIMIZATION IN CIVIL ENGINEERING
Int. J. Optim. Civil Eng., 2017; 7(2):291-318

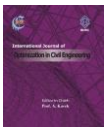

NONLINEAR FRAME ANALYSIS BY MINIMIZATION TECHNIQUE

M. Rezaiee-Pajand[*, †] and R. Naserian
Civil Engineering Department, Ferdowsi University of Mashhad, Mashhad, Iran

ABSTRACT

By minimizing the total potential energy function and deploying the virtual work principle, a higher-order stiffness matrix is achieved. This new tangent stiffness matrix is used to solve the frame with geometric nonlinear behavior. Since authors' formulation takes into account the higher-order terms of the strain vector, the convergence speed of the solution process will increase. In fact, both linear and nonlinear parts of the frame axial strains are included in the presented formulation. These higher-order terms affect the resulting unbalanced force and also frame tangent stiffness. Moreover, the finite element method, updated Lagrangian description, and arc length scheme are employed in this study. To check the efficiency of the proposed strategy, several numerical examples are solved. The findings indicate that the authors' technique can accurately trace the structural equilibrium paths having the limit points.

Keywords: nonlinear axial strain; tangent stiffness; planar frame; nonlinear analysis; updated Lagrangian; arc length scheme.

Received: 16 September 2016; Accepted: 21 November 2016

1. INTRODUCTION

Because of the economic consideration, some frames are built more flexible nowadays. For these cases, accurate considerations in the analysis and design are required. All structures which deform largely, they behave nonlinearly prior to reaching to their ultimate strength. There are two different types of the nonlinear behavior in the structures, namely the material and geometrical nonlinear performance. In the former, the stress and strain are nonlinearly related. This is due to properties of the structural martial. In another case; the structure's geometry changes due to the large deformations. As a result, the stiffness matrix should be set up in each step of the analysis, based on the corresponding deformations. Up to now,

[*]Corresponding author: Civil Engineering Department, Ferdowsi University of Mashhad, Mashhad, Iran
[†]E-mail address: rezaiee@um.ac.ir (M. Rezaiee-Pajand)

extensive researches have been conducted to present an appropriate stiffness matrix which is capable of achieving the equilibrium path of structures. The behavior of structures under the load is dependent on the various factors. To find accurate results, all of these parameters should be included in the stiffness matrix.

Safaan proposed the first geometric nonlinear stiffness matrix of frames by using simple formulas. However, this technique did not lead to the acceptable results [1]. Afterwards, researchers suggested the stiffness matrices with the help of Lagrangian techniques. For nonlinear analysis of structures, three general descriptions are usually presented, for considering the body's configuration. In the first approach, which is named total Lagrangian, the initial shape of the member, which is called the base configuration, is used in the analysis [2]. Note that the last available position of element is considered as the reference shape in the updated Lagrangian method [3]. The third strategy deploys the rigid body motions and infinitesimal deformations [4]. This scheme is named co-rotational tactic. It should be reminded that the updated Lagrangian technique is more accurate and efficiency than the total Lagrangian [5] and [6]. For this reason; the updated Lagrangian is employed in this study.

Conner used a simple stiffness matrix which was applicable in limited situations [7]. This investigator utilized a shape function for the member, which was previously introduced by Powell [8]. The mentioned frame member had small deformations, having the axial force and flexural moments at its ends. Afterwards, Oran formulated the symmetric stiffness matrix for the members with axial-flexural behavior [9] and [10]. This matrix was constructed based on the updated Lagrangian approach. In another event, Yang analyzed the frames and beams with the help of simple formulas [11]. He took advantage from the strain energy function, and constructed the stiffness matrix, for the small deformation members. Wen and Rahimzadeh proposed a formulation for the analysis of the frames, by considering the small nodal rotation, large transmission and rotation of the members [12]. Based on these assumptions, the element motions were estimated by using a third-order function. Note that the obtained tangent matrix is suitable for the small deformations and cannot work in the case of large displacements. By applying the virtual work principle and using some nonlinear terms of strain, the stiffness matrix of the beams twisted non-uniformly was explored by Yang and McGuire [13].

In another study, Spillers calculated the asymmetric stiffness matrix of the space frames with large rotations and small rotational strain [14]. This matrix is unsuitable for the buckling problems. In order to analyze the plane frames with small strain and moderate to large rotation, second-order effects for geometrically nonlinear behavior were considered by Torkamani *et al.* [15]. As a result, a symmetric matrix which is the sum of four matrices was achieved. Furthermore, two matrices of the second-order included the displacement components. Chang obtained the higher-order stiffness matrix of the space frames by the usage of the rigid body rule [16]. This matrix is divided into three sections of elastic, geometric and higher-order terms. It is worth emphasizing; the parameters that the make up the geometric and higher-order stiffness matrices have force components. Yang *et al.* employed the geometric stiffness of the curved beams in buckling analysis [6]. The higher-order stiffness matrices of the truss structures were formulated by Torkamani and Shieh [17] and also by Rezaiee-Pajand and Naserian [18]. By considering the large deformations, all the linear and nonlinear terms of the strain were taken into account in equilibrium equations.

Consequently, an asymmetric matrix with five parts calculated. Gorgun and Yilmaz [19] and Gorgun [20] investigated the geometrical nonlinear behavior of plane frames with semi-rigid and flexible connections, respectively. By using the minimization of difference between the measured and analytical static displacement, a novel algorithm for the static damage detection of frame structures was obtained by Rezaiee-Pajand *et al.* [21]. Based on the exact solution of governing differential equations, Rezaiee-Pajand *et al.* computed the critical buckling load of the semi-rigid steel frames with members [22-23]. In another research, the nonlinear behavior of the material and geometrical of the shear-flexible frame problems were investigated [24].

Based on the review of the other investigator papers, it can be deduced that sufficient studies have not been done for developing a robust frame tangent stiffness, so far. In fact, some researchers neglected the higher-order terms of the strains in the two-dimensional frame analysis. In this study, both linear and nonlinear parts of the frame axial strains are included in the formulation. These higher-order terms affect the resulting unbalanced force and also frame tangent stiffness. As a result, better convergence speed of the solution process will be achieved. To test the ability and efficiency of the authors' techniques, various numerical problems will be solved. The outcomes of these geometric nonlinear analyses will be also compared with the answers of the former investigators.

2. HIGHER-ORDER STIFFNESS MATRIX

In this paper, a new higher-order stiffness matrix will be formulated for geometric nonlinear analysis of the plane frames. The following assumptions will be used in the mathematical calculation process.

2.1 Assumptions

In order to solve the problems more effectively, the coming assumptions are considered:

1. The members of the structure are straight. Additionally, no imperfection and residual stress exist among the elements.
2. The cross sections of the members are symmetric about the principal axes. Moreover, the centroid axis of the cross section is in direction of the element longitudinal axis.
3. The structural deformations occur only in the members' plane. Additionally, the local buckling is negligible.
4. The cross sections of structural members always remain plane. Afterward, the cross sections remain perpendicular to the longitudinal axes though the members' deformation.
5. The distributed loads are applied to the symmetry axis of the cross section.

2.2 Finite element method

A plane frame element is demonstrated in Fig. 1. This member has six degrees of freedom, and the nodal displacement vector has the following shape:

$$\{d\}^T = \{u_1, v_1, \theta_1, u_2, v_2, \theta_2\} \tag{1}$$

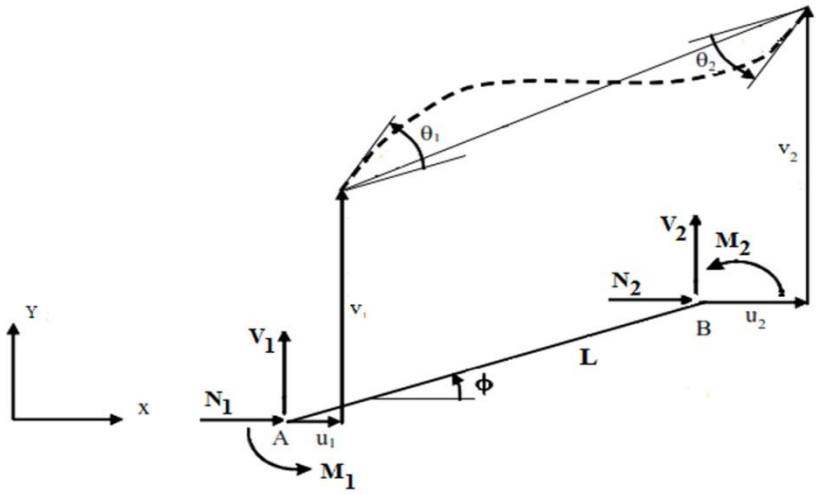

Figure 1. Coordinate systems of a plane frame element

where, u_1, v_1, Θ_1 and u_2, v_2, Θ_2 are referred DOFs corresponding to translations of node 1 and 2 along the directions of x, y and z, respectively. The nodal force vector can be written as below:

$$\{f\}^T = \{N_1, V_1, M_1, N_2, V_2, M_2\} \tag{2}$$

Here, N_1, V_1, M_1 and N_2, V_2, M_2 are the components of force corresponding to node 1 and 2 along the directions of x, y and z, respectively. It should be reminded that the displacements of an arbitrary point placed on the cross section can be expressed in terms of the deformations of the neutral axis as follows [15]:

$$u = u_0 - y\frac{dv}{dx}, v = v_0 \tag{3}$$

In this equation, u_0, v_0 and u, v are the displacements of the cross section's center and arbitrary point in the directions of x and y, respectively. Furthermore, the vertical distance of the selected arbitrary point from the neutral axis is shown by y.

For relationship between the motions of an arbitrary point and nodal displacements, the following shape functions will be used:

$$u_0(x) = [N_u]\{d\} \tag{4}$$
$$v_0(x) = [N_v]\{d\} \tag{5}$$
$$\theta_0(x) = [N_\theta]\{d\} \tag{6}$$

In the last relation, $[N_u]$, $[N_v]$ and $[N_\theta]$ denote the vectors of shape functions for the axial, vertical displacement and rotation of a frame member, respectively. Using the

equilibrium conditions of the straight beam with nodal moments leads to the subsequent third-order equation for vertical displacement:

$$EI\frac{d^2v}{dx^2} = M_1(1-\frac{x}{L}) + M_2\frac{x}{L} \tag{7}$$

$$v = a_0 + a_1x + a_2x^2 + a_3x^3 \tag{8}$$

In this relationship, E and I are the modulus of elasticity and the moment of inertia, respectively. The shape functions of the axial and rotational deformations can be obtained by deploying a linear relation as follows:

$$u = b_0 + b_1x \quad , \quad \theta = c_0 + c_1x \tag{9}$$

According to the Fig. 1, the following are the boundary conditions of the plane frame element:

$$\begin{cases} x = 0, \quad u = u_1, \quad v = v_1, \quad \theta = \theta_1, \quad \dfrac{dv}{dx} = \theta_1 \\ x = L, \quad u = u_2, \quad v = v_2, \quad \theta = \theta_2, \quad \dfrac{dv}{dx} = \theta_2 \end{cases} \tag{10}$$

Utilizing the boundary conditions stated in Eq. (10) leads to shape functions in the coming form:

$$[N_u] = \left[1-\frac{x}{L}, 0, 0, \frac{x}{L}, 0, 0\right] \tag{11}$$

$$[N_v] = \left[0, 1-\frac{3x^2}{l^2}+\frac{2x^3}{l^3}, x-\frac{2x^2}{l}+\frac{x^3}{l^2}, 0, \frac{3x^2}{l^2}-\frac{2x^3}{l^3}, -\frac{x^2}{l}+\frac{x^3}{l^2}\right] \tag{12}$$

$$[N_\theta] = \left[0, 0, 1-\frac{x}{L}, 0, 0, \frac{x}{L}\right] \tag{13}$$

2.3 Equilibrium equations

By minimizing the total potential energy function and deploying the virtual work principle, the coming incremental equilibrium equation can be achieved:

$$\delta(\Delta\Pi) = \delta(\Delta U) - \delta(\Delta W) = 0 \tag{14}$$

In this equality, the strain energy and the external potential work are demonstrated by U and W, respectively. Moreover, σ and ε denote the axial stress and strain, respectively. The axial stress of the member has the next form:

$$\delta(\Delta U) = \delta(\frac{1}{2}\int \sigma\, \varepsilon\, dv) \tag{15}$$

$$\delta(\Delta W) = \{\delta d\}^T \{f\} \tag{16}$$

$$\sigma = \sigma_0 + E\, \varepsilon \tag{17}$$

In this relationship, σ_0 is the axial stress in the reference shape. The axial strain of the frame element can be divided into linear and nonlinear parts [25]. The frame element's strain has the succeeding appearance:

$$\varepsilon_{xx} = e_{xx} + \eta_{xx} \tag{18}$$

The linear and the nonlinear parts of the strain are shown by e_{xx} and η_{xx} respectively. Inserting Eqs. (15)-(18) into Eq. (14) leads to the incremental static equation, which can be expressed as below:

$$\begin{aligned}\delta(\Delta\Pi) = &\int_v E e_{xx}\delta e_{xx} dv + \int_v E\eta_{xx}\delta e_{xx} dv + \int_v E e_{xx}\delta\eta_{xx} dv + \\ &\int_v E\eta_{xx}\delta\eta_{xx} dv + \int_v \sigma_0 \delta e_{xx} dv + \int_v \sigma_0 \delta\eta_{xx} dv - \{\delta d\}^T\{f\} = 0\end{aligned} \tag{19}$$

By utilizing Eqs. (3)-(5), the linear and nonlinear parts of the strain can be achieved in the coming form:

$$e_{xx} = \frac{du}{dx} = \frac{du_0}{dx} - y\frac{d^2 v_0}{dx^2} = [N_u']\{d\} - y[N_v'']\{d\} \tag{20}$$

$$\begin{aligned}2\eta_{xx} = &(\frac{du}{dx})^2 + (\frac{dv}{dx})^2 = (\frac{du_0}{dx} - y\frac{d^2 v_0}{dx^2})^2 + (\frac{dv_0}{dx})^2 = \\ &\{d\}^T[N_u']^T[N_u']\{d\} + y^2\{d\}^T[N_v'']^T[N_v'']\{d\} - \\ &2y\{d\}^T[N_u']^T[N_v'']\{d\} + \{d\}^T[N_v']^T[N_v']\{d\}\end{aligned} \tag{21}$$

The differential equations of linear and nonlinear strain can be obtained as:

$$\delta e_{xx} = \{\delta d\}^T[N_u'] - y\{\delta d\}^T[N_v''] \tag{22}$$

$$\begin{aligned}\delta\eta_{xx} = &\{\delta d\}^T[N_u']^T[N_u']\{d\} + y^2\{\delta d\}^T[N_v'']^T[N_v'']\{d\} - \\ &2y\{\delta d\}^T[N_u']^T[N_v'']\{d\} + \{\delta d\}^T[N_v']^T[N_v']\{d\}\end{aligned} \tag{23}$$

$$[N'] = \frac{dN}{dx} \tag{24}$$

In which, $\lfloor N' \rfloor$ includes the derivatives of the shape functions with respect to x parameter. By applying Eqs. (20)-(23), the incremental equilibrium Eq. (19) can be rewritten

in the below shape:

$$\begin{aligned}
&\delta(\Delta\Pi) = \{\delta d\}^T \int_v E\,([N'_u]^T - y[N''_v]^T)([N'_u] - y[N''_v])\{d\}dv + \\
&\{\delta d\}^T \int_v \frac{E}{2}([N'_u]^T - y[N''_v]^T)(\{d\}^T[N'_u]^T[N'_u] + y^2\{d\}^T[N''_v]^T[N''_v] - \\
&2y\{d\}^T[N'_u]^T[N''_v] + \{d\}^T[N'_v]^T[N'_v])\{d\}dv + \{\delta d\}^T \int_v E\,([N'_u]^T[N'_u]\{d\} + \\
&y^2[N''_v]^T[N''_v]\{d\} - 2y[N'_u]^T[N''_v]\{d\} + [N'_v]^T[N'_v]\{d\})([N'_u] - y[N''_v])\{d\}dv + \\
&\{\delta d\}^T \int_v \frac{E}{2}([N'_u]^T[N'_u] + y^2[N''_v]^T[N''_v] - 2y[N'_u]^T[N''_v] + \\
&[N'_v]^T[N'_v])\{d\}\{d\}^T([N'_u]^T[N'_u] + y^2[N''_v]^T[N''_v] - 2y[N'_u]^T[N''_v] + \\
&[N'_v]^T[N'_v])dv + \{\delta d\}^T \int_v \sigma_0([N'_u]^T dv - y[N''_v]^T)dv + \{\delta d\}^T \int_v \sigma_0([N'_u]^T[N'_u] + \\
&y^2[N''_v]^T[N''_v] - 2y[N'_u]^T[N''_v] + [N'_v]^T[N'_v])\{d\}dv - \{\delta d\}^T\{f\} = 0
\end{aligned} \tag{25}$$

2.4 Components of the stiffness matrix

The incremental equilibrium Eq. (25) can be written in the next form:

$$\delta(\Delta\Pi) = \{\delta d\}^T[K]\{\delta d\} - \{\delta d\}^T\{f\} = 0 \tag{26}$$

By deploying this equality, the higher-order stiffness matrix of the frame element can be obtained in the following shape:

$$[K_L] = [K_0] + [K_P] + \frac{1}{2}[K_1] + [K_2] + \frac{1}{2}[K_3] \tag{27}$$

In this relation, the next matrices are used:

$$[K_0] = \int_l EA[N'_u]^T[N'_u]dx + \int_l EI[N''_v]^T[N''_v]dx \tag{28}$$

$$\begin{aligned}
[K_P] = P\int_l ([N'_u]^T[N'_u] + [N'_v]^T[N'_v])dx + \\
P\frac{I}{A}\int_l ([N''_v]^T[N''_v])dx + 2\int_l M([N'_u]^T[N''_v])dx
\end{aligned} \tag{29}$$

$$\begin{aligned}
[K_1] = EA\int_l [N'_u]^T(\{d\}^T[N'_u]^T[N'_u] + \{d\}^T[N'_v]^T[N'_v])dx + \\
EI\int_l [N'_u]^T(\{d\}^T[N''_v]^T[N''_v])dx + 2EI\int_l [N''_v]^T(\{d\}^T[N'_u]^T[N''_v])dx
\end{aligned} \tag{30}$$

$$[K_2]=EA\int_l([N'_u]^T[N'_u]+[N'_v]^T[N'_v])(\{d\}[N'_u])dx+$$
$$EI\int_l([N''_v]^T[N''_v])(\{d\}[N'_u])dx+2EI\int_l([N'_u]^T[N''_v])(\{d\}[N''_v])dx \quad (31)$$

$$[K_3]=EA\int_l([N'_u]^T[N'_u]+[N'_v]^T[N'_v])\{d\}\{d\}^T([N'_u]^T[N'_u]+[N'_v]^T[N'_v])dx+$$
$$EI\int_l([N'_u]^T[N'_u]+[N'_v]^T[N'_v])\{d\}\{d\}^T([N''_v]^T[N''_v])dx+$$
$$EI\int_l([N''_v]^T[N''_v])\{d\}\{d\}^T([N'_u]^T[N'_u]+[N'_v]^T[N'_v])dx+ \quad (32)$$
$$4EI\int_l([N'_u]^T[N''_v])\{d\}\{d\}^T([N'_u]^T[N''_v])dx+$$
$$EI_2\int_l([N''_v]^T[N''_v])\{d\}\{d\}^T([N''_v]^T[N''_v])dx$$

$$\int_A dA=A,\quad \int_A\sigma_0 dA=P,\quad \int_A\sigma_0 ydA=-M,\quad \int_A\sigma_0 y^2dA=P\frac{I}{A} \quad (33)$$

In these equalities, the axial force and bending moment are shown by P and M, respectively. The element's bending moment can be expressed in terms of nodal bending moments as follows:

$$M=M_1(1-\frac{x}{L})+M_2(\frac{x}{L}) \quad (34)$$

Eq. (25) includes the integration of the fourth-order for the y parameter. In this paper, the second moment of inertia is defined in the coming shape:

$$\int_A y^4dA=I_2 \quad (35)$$

This factor is placed in the last term of the matrix $[K_3]$. The second moment of inertia is only depended on the shape and size of the cross section. It should be reminded that $\int_A ydA$ and $\int_A y^3dA$ equal to zero, due to the symmetry assumption of the members` cross section.

In these relationships, the element stiffness matrix $[K_L]$ has five different parts. The elastic and geometric stiffness of the member are demonstrated by $[k_0]$ and $[K_P]$, respectively. In contrast to the constant elastic stiffness matrix, the geometric stiffness matrix is depended on the axial force. The three remaining pieces are the member higher-order matrices. The linear terms of the element's incremental displacements are placed into $[K_1]$ and $[K_2]$ matrices. On the other hand, $[K_3]$ is in terms of the second-order functions of

the incremental deformations. All the higher-order matrices will be given in appendix A.

Recall that the stiffness matrix stated in Eq. (27) is obtained based on local coordinates. By employing the transformation matrix, it can be transformed to the global coordinates. The following relation shows the process in which the local stiffness matrix converts into the global one:

$$[K_e] = [T]^T [K_L][T] \tag{36}$$

In this equality, $[K_e]$ and [T] are the global stiffness matrix and transformation matrix, respectively. The transformation matrix converts the member stiffness from local coordinates into the global ones. It should be added that the transformation matrix of the plane frame structures will be given in appendix B. In the well-know process; the total nonlinear stiffness matrix of the structure can be obtained by assembling the global incremental stiffness matrices of the members.

3. SOLVING NONLINEAR EQUATIONS

The structural analysis aims to find the response of equilibrium equation, which governs the behavior. This relation has the coming shape:

$$\{F\} = [K]\{D\} \tag{37}$$

In the last relationship, the force vector, global nonlinear stiffness matrix and nodal displacement vector are shown by {f}, [K] and {D}, respectively. To achieve the nonlinear structural equilibrium path, three methods are proposed for solving Eq. (37). These are called the pure incremental approach, incremental- iterative tactic and direct technique. In the pure incremental scheme, the static path is obtained by deploying linear approximations. The related simplifications may lead to divergence of the solution [26]. Although this strategy is easy, its application is limited. For instances, the mentioned approach may not reach to the exact responses, in problems with large deformations [27].

In the direct algorithm, only one load increment exists. In this method, by using secant stiffness matrix the iterative procedures are carried out to obtain the equilibrium path. Note that the aforesaid tactic is only practical in the structures with moderate displacements [28]. According to experiences, the most efficient strategy for analyzing the nonlinear structures is the iterative-incremental method. In this scheme, each loading step is divided into two sections: 1- predictor step 2- iterative step. In the former stage, the displacement is, firstly, approximated by specifying the load factor. In the latter stage, the successive iterative procedure is conducted for obtaining the static path.

It should be reminded, one of the classical techniques, which is very common is named Newton-Raphson. Note that the loading level remains constant in each step of this load control tactic [29]. This way has a low speed. In fact, the stiffness matrix is updated for numerous times in the Newton-Raphson procedure. To remedy these drawbacks, Crifield introduced the updated Newton-Raphson algorithm [30]. Additionally, the Newton-Raphson schemes perform weakly in encountering load limit points. To solve this difficulty,

displacement control method was suggested [31]. In this technique, one specific displacement component is presumed to be constant in each incremental step. It is worth mentioning; this strategy leads to inaccurate responses in problems with snap back behavior.

Other nonlinear solvers, named arc length techniques, were, firstly, presented by [32] and [33]. Constraint equation of these methods indicates the distance of the last point placed on the equilibrium path from the path obtained through iterative analyses. In the normal plane strategy, location of the iterative points is normal to the tangent passing through the previous static point [34]. The vector passing through the iterative and previous equilibrium point is perpendicular to the locus of the iterative points in the updated normal plane technique [35]. Another well-known scheme utilized in the nonlinear structural analysis is cylindrical arc length method. By disregarding the load component with respect to displacements one in constraint equation, Riks's improved technique was obtained [36]. Other forms of the nonlinear solvers were suggested by minimizing some parameters, such as reduced unbalanced load vector, residual displacement, perimeter and area [37-39].

Moreover, the new two-point strategy was utilized for nonlinear analysis of structures [40] and [41]. Furthermore, Saffari proposed the three-point approach with the eight-order convergence by inserting the effective functions into the normal flow algorithm [42]. In addition, the geometric and material inelastic nonlinear analysis of the space trusses was carried out [43]. For analyzing the nonlinear pre-buckling behavior, four systematic approaches were utilized [44]. An iterative procedure to solve the linear system of equations was implemented instead of computing the inversion of the tangent stiffness matrix. By minimizing the residual displacement, the analysis of structures with severe nonlinear behavior was performed [45]. Recently, the dynamic relaxation approach was applied by Rezaiee-Pajand and Estiri [46-49], for obtaining the equilibrium paths and the limit points of structures.

In this paper, the cylindrical arc length method along with higher-order stiffness matrix will be employed for more rapid nonlinear analysis of the frame structures. In the following subsections, the formulation of this strategy will be presented by using the update Lagrangian description.

3.1 Cylindrical arc length technique

The solution procedure related to the cylindrical arc length method is demonstrated in Fig. 2. By considering the (n-1)th static point, the analysis is carried out to specify the n-th point on the equilibrium path. Firstly, the incremental load is obtained at the predictor stage. To achieve the corresponding displacement the subsequent system of equation should be solved:

$$K^{n-1}\Delta D_1^n = \Delta\lambda_1^n P \tag{38}$$

In this equation, the tangent stiffness matrix related to the (n-1)th static point is denoted by K^{n-1}. Moreover, $\Delta\lambda_1^n$ is incremental load factor in the nth step. Employing Eq. (38) leads to the coordinates of the point 1. Since this point is not placed on the equilibrium path, the successive iterations should be carried out. In all iterations of the cylindrical arc length method, the distance between the response points of the iterative steps and the previous

static point is equal to a constant quantity of arc length (L_n).

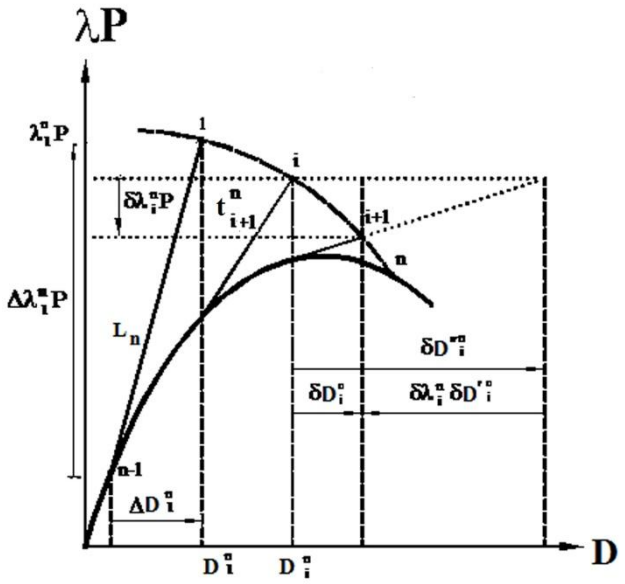

Figure 2. The solution procedure of the arc length tactic

Based on the Fig. 2, the constraint equation can be expressed as follows:

$$t_{i+1}^{n} \cdot t_{i+1}^{n} = (L_n)^2 \tag{39}$$

By ignoring the load component [36], the constraint equation is simplified as below:

$$\Delta D_{i+1}^{n\ T} \Delta D_{i+1}^{n} = (L_n)^2 \tag{40}$$

This equality can be rewritten in the coming shape:

$$\left(\Delta D_i^n + \delta D_i^n\right)^T \left(\Delta D_i^n + \delta D_i^n\right) = (L_n)^2 \tag{41}$$

In each iteration, the displacement has the next form:

$$\delta D_i^n = \delta D_i''^n + \delta\lambda_i^n \delta D_i'^n \tag{42}$$

Where, the displacements corresponding to the residual load, R, and the external force, P, are shown by $\delta D_i''^n$ and $\delta D_i'^n$, respectively. The subsequent relationships can be used to calculate these displacements:

$$K_i^n \delta D_i''^n = R_i^n \tag{43}$$

$$K_i^n \delta D_i'^n = P \tag{44}$$

As it will be demonstrated in Appendix A, three higher-order matrices shown by $[K_1]$, $[K_2]$ and $[K_3]$ are linear and nonlinear functions of the incremental displacements. Consequently, the variant stiffness matrix is updated at each iteration step. Based on Fig. 2, the residual force of the n-th iteration (R_i^n) is computed by employing the following equation:

$$R_i^n = \lambda_i^n P - F_i^n \tag{45}$$

In this equality, F_i^n denotes the nodal force in the n-th iteration. Because the residual load and the external force are known at the beginning of each iteration, the system of Eqs. (43)-(44) can be solved. Hence, based on Eq. (42), only $\delta\lambda_i^n$ is required for computing δD_i^n . In iteration steps, inserting Eqs. (42)-(44) into Eq. (41) and simplifying leads to the subsequent second-order relationship:

$$\alpha(\delta\lambda_i^n)^2 + \beta(\delta\lambda_i^n) + \gamma = 0 \tag{46}$$

The constant parameters of this relation have the coming shape:

$$\alpha = \delta D_i'^{nT} \delta D_i'^n \tag{47}$$

$$\beta = 2\left(\Delta D_i^n + \delta D_i''^n\right)^T \delta D_i'^n \tag{48}$$

$$\gamma = \left(\Delta D_i^n + \delta D_i''^n\right)^T \left(\Delta D_i^n + \delta D_i''^n\right) - \left(L_n\right)^2 \tag{49}$$

After specifying these constants and solving Eq. (46), two roots of this relationship can be achieved in the next form:

$$(\delta\lambda_i^n)_{1,2} = -\frac{\beta}{2\alpha} \pm \sqrt{(\frac{\beta}{2\alpha})^2 - \frac{\gamma}{\alpha}} \tag{50}$$

Three following cases can be considered for these roots:

$$\beta^2 - 4\alpha\gamma > 0 \tag{51}$$

$$\beta^2 - 4\alpha\gamma = 0 \tag{52}$$

$$\beta^2 - 4\alpha\gamma < 0 \tag{53}$$

At the first case, both answers are real. The root, whose distance from the previous iteration point is minimum, can be selected as the acceptable response. This scheme prevents the static path from returning to itself. When Eq. (52) equals zero, only one acceptable root

exists. In last case, the roots are virtual and unsuitable. Consequently, the arc length (L_n) should be reduced, and the solution procedure must be repeated.

4. NUMERICAL EXAMPLES

To investigate the efficiency and ability of the novel technique, some frame structures with geometric nonlinear behavior will be solved. The obtained responses will be compared with the available results, for proving the accuracy of the new formulations. It should be added that several plane frames with various cross sections have been analyzed by the authors, and a few of these structures will be presented in the subsequent subsections.

4.1 Fixed beam

Fig. 3 shows a fixed-fixed beam with rectangular cross section. For evaluation, the real behavior of this symmetric structure, it was tested under an increasing central vertical load by El-Ghazaly and Monforton [50]. The elasticity modulus of beam is E=20692.5 kN/cm^2. As it is shown in Fig. 3, the area cross section, and moment of inertia are A=1.62 cm^2 and I=0.055cm^4, respectively. In the solution process, a unit arc length will be employed in the loading steps.

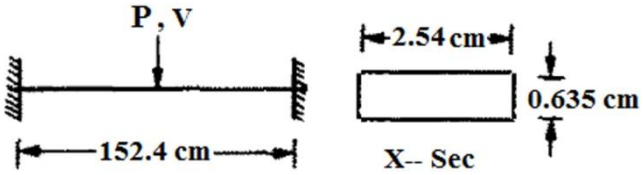

Figure 3. Fixed-fixed beam

The second moment of inertia for the rectangular cross section can be computed with help of the following equation:

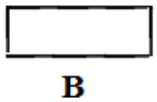

$$I_2 = \int_A y^4 dA = \int_{-\frac{H}{2}}^{\frac{H}{2}} y^4 (B dy) = B\left(\frac{y^5}{5} \right]_{-\frac{H}{2}}^{\frac{H}{2}} = \frac{BH^5}{160} \tag{54}$$

$$I_2 = \frac{2.54 \times 0.64^5}{160} = 0.0017\ cm^6 \tag{55}$$

By using the authors' algorithm, the higher-order nonlinear analysis of this structure will be carried out. Fig. 4 shows the obtained results for the fixed beam. To demonstrate the validity, the findings are compared with El-Ghazaly's numerical [50] and experimental responses in the same Fig.

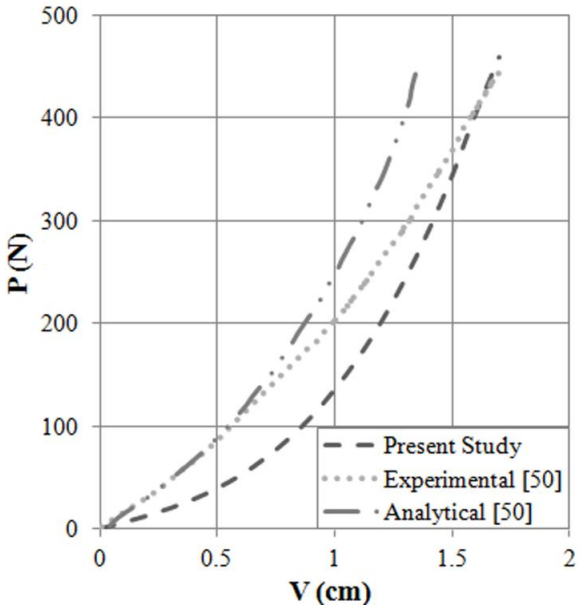

Figure 4. The equilibrium path of the Fixed- fixed beam

According to the Fig. 4, by considering all the linear and nonlinear components of the strain vector, the new tactic can trace the structural path more accurate.

4.2 Williams toggle frame

As it is illustrated in Fig. 5, two members of the toggle frame have the angle of 1.7 with respect to the horizon. At first, this structure was analyzed and experimentally investigated by Williams [51]. In another study, Wood and Zienkiewicz employed finite element method for analyzing this frame with rectangular cross section [52]. Moreover, by using the residual displacement procedure, the behavior of Williams's toggle frame was studied with circular cross section by Chan [38]. Due to rather complex and interesting behavior, this plane structure was investigated intensively, by using other nonlinear solution strategies, by Rezaiee-Pajand and Alamatian [53, 54]] and Rezaiee-Pajand *et al.* [55, 56].]. In this paper, toggle frame with rectangular [52], circular [38] and hollow cross section, which is proposed by the authors, is analyzed. The employed cross sections are shown in the Fig. 5.

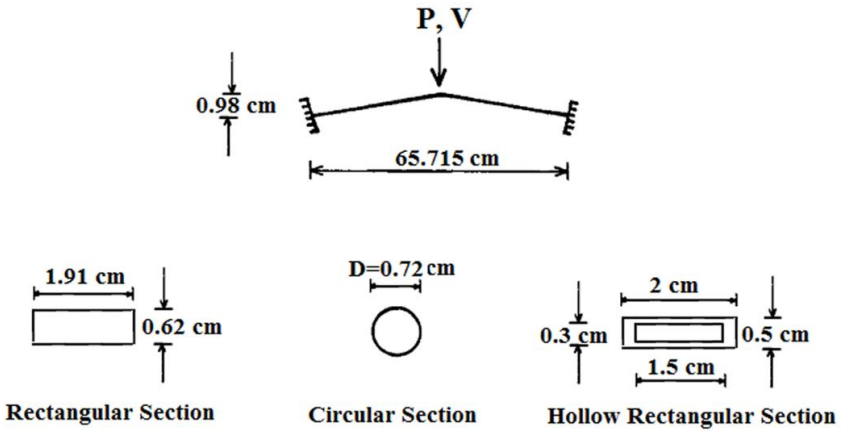

Figure 5. Williams toggle frame

A unit concentrated load is applied to the top of the frame. Furthermore, the arc length in the loading steps is assumed 1. The second moment of inertia of the circular cross section is obtained as below:

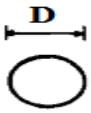

$$I_2 = \int_A y^4 dA = \int\int (r\sin\theta)^4 (r dr\, d\theta) = \int_0^{2\pi} (\sin\theta)^4\, d\theta \int_0^{\frac{D}{2}} r^5 dr = \frac{\pi D^6}{512} \tag{56}$$

$$I_2 = \frac{\pi \times 0.72^6}{512} = 0.00085\ cm^6 \tag{57}$$

The axial, first and the second flexural rigidity of the members are listed in Table 1:

Table 1: Properties of toggle frame

Section	Axial Rigidity (EA) kN	Flexural Rigidity (EI) kN.Cm^2	Second Flexural Rigidity (EI_2) kN.Cm^4
Rectangular	8369	268.5	7.8
Circular	8134.6	263.6	11.7
Hollow Rectangular	7578.7	240.6	5.1

This structure with rectangular, circular and hollow cross section having nonlinear behavior is analyzed. Fig. 6 illustrates the obtained responses and the results of two other researchers' works. It is obvious that the load-displacement diagram of this frame includes a snap-through part. Based on the Fig. 6, the authors' tactic possesses the ability of passing the limit point of the equilibrium path. Moreover, the proposed method reaches to the load limit point after tracing the longer path in comparison with predecessors' tactic. Consequently, the new higher-order nonlinear technique is more accurate than the other strategies.

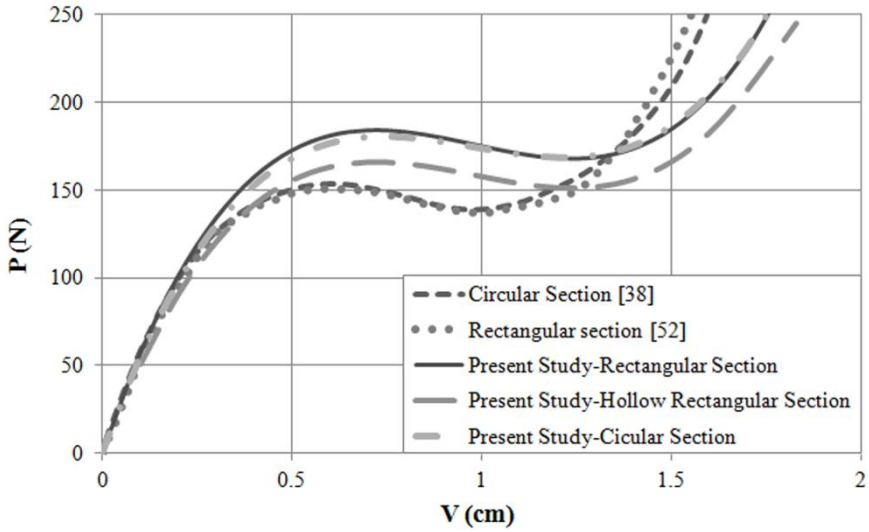

Figure 6. The equilibrium path of the Toggle frame

4.3 Five-story frame

Fig. 7 shows the geometry and loading of the 29-member frame. This five-story structure was analyzed before by using the dynamic relaxation method [57] and [58], and also the optimization schemes [59]. The beams and columns are W18×35 and W21×50, respectively. The elasticity modulus of all members is 2×10^8 kN/m^2. Moreover, the arc length in the loading steps is assumed to be five.

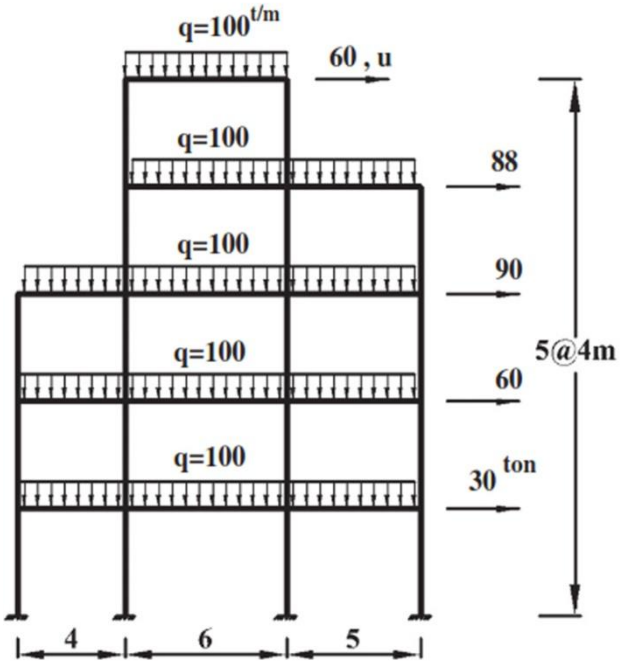

Figure 7. Five-story frame

It should be added that a novel parallel axis theorem is utilized for calculation of the second moment of inertia for the compound cross sections. This rule is formulated as below:

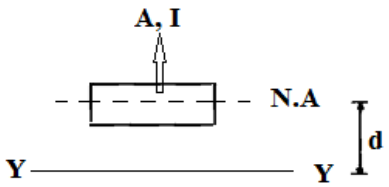

$$I_{2(y-y)} = I_{2\,N.A} + Ad^4 + 6d^2 I^2 \tag{58}$$

In this equation, $I_{2(y-y)}$ and $I_{2(N.A)}$ are the second moment of inertia about an arbitrary and natural axis, I is the moment of inertia about the natural axis, and d is the distance of two axes.

Solving Eq. (58) leads to coming results for the second moment of inertia in Table 2.

Table 2: Properties of the five-story frame's members

Member	Section	Area Section (A) Cm^2	Moment of Inertia (I) Cm^4	Second Moment of Inertia (I_2) Cm^6
Beam	W18×35	66.45	21227.8	8321638.1
Column	W21×50	94.84	40957.17	21779797.12

The equilibrium path of the plane frame is shown in Fig. 8. Note that the distributed load is converted to the nodal moment and vertical loads before the analysis. Based on the static path, utilizing the higher-order stiffness matrix leads to the results compatible with the other studies.

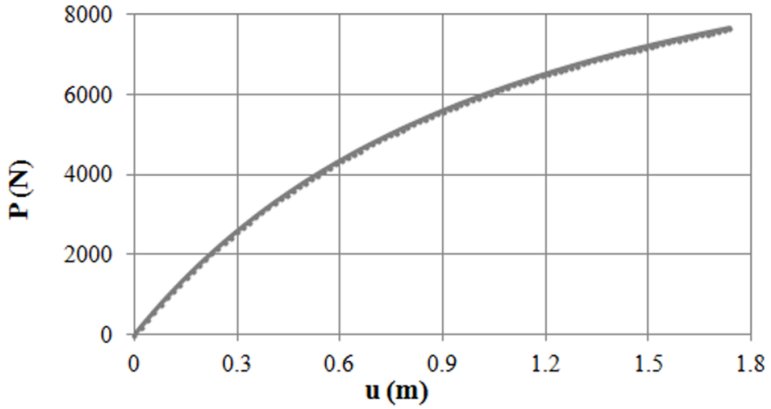

Figure 8. The equilibrium path of the five- story frame

4.4 Gable frame

In this part of the paper, a more accurate nonlinear analysis of the gable frame proposed by the authors is carried out. This frame with four cross sections is demonstrated in Fig. 9. A concentrated load of one kN is applied at the head of structure. The elasticity modulus of the members equals to 20500 kN/cm^2. Furthermore, a unit length increment factor is used in load steps.

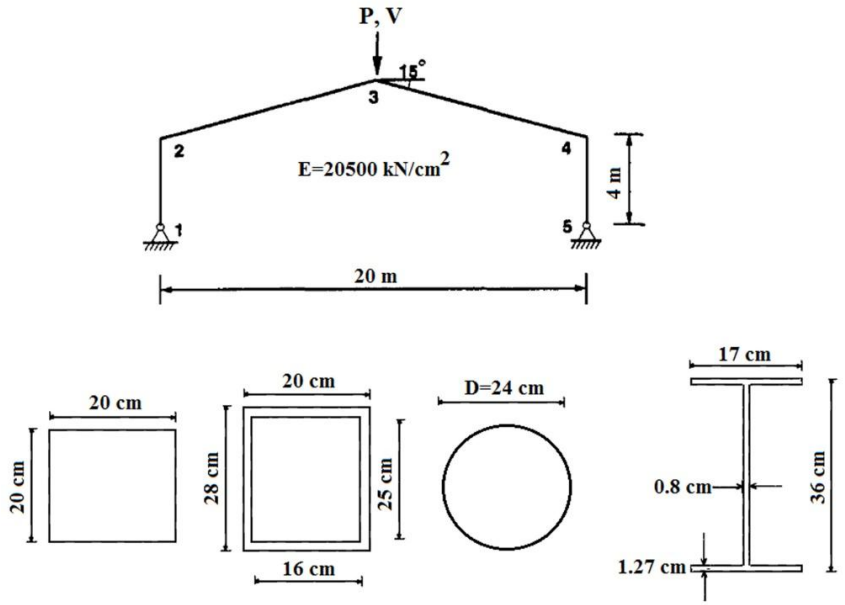

Figure 9. Gable frame

The properties of the cross sections of members are listed in Table 3.

Table 3: Properties of the gable frame's members

Section	Area Section (A) Cm^2	Moment of Inertia (I) Cm^4	Second Moment of Inertia (I_2) Cm^6
Rectangular	400	13333	400000
Hollow Rectangular	160	15753	1174734
Circular	452.4	16286	1172593
IPE 360	72.7	16270	4166457

This gable frame is analyzed four times by utilizing rectangular, hollow rectangular, circular and IPE cross sections. The corresponding equilibrium paths are shown in Fig. 10. It is obvious that the static paths are obtained accurately. As it is shown in the Fig. 10, three detected equilibrium paths, which are found by employing I-shaped, circular and hollow cross sections, are the same. Whereas, the curve related to the rectangular cross section is below the other cross sections' ones. This is because the moment of inertia and the second moment of inertia of the rectangular cross section is less, in comparison with other cross sections used in this example.

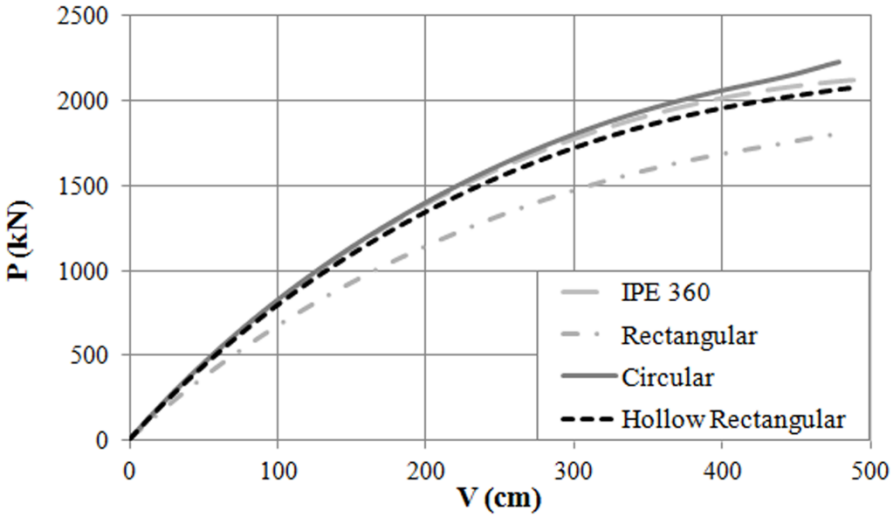

Figure 10. The equilibrium path of the gable frame

5. CONCLUSION

Some flexible frames experience large displacements under the loads or special boundary conditions. Based on the virtual work principle, a robust tangent stiffness matrix is achieved by minimizing the total potential energy. All terms of the strain vector are taken into account in the equilibrium equations. In the next stage, the cylindrical arc length approach is applied for solving the nonlinear governing equations. This nonlinear solver uses the presented frame stiffness matrix. To demonstrate the ability of the new formulations, and also implement the authors' computer program, some geometric nonlinear analyses are performed by solving various examples. Findings prove that employing the novel technique lead to the outcomes, which are compatible with the other researchers' experimental and numerical results. In addition, the present tangent stiffness matrix gives more accurate answers, in comparison with the previously published solutions.

APPENDIX A

The elastic stiffness matrix $[K_0]$, the geometric stiffness matrix $[K_p]$, and the higher-order stiffness matrices $[K_1]$, $[K_2]$, and $[K_3]$ of the plane frame are given below:

It is worth emphasizing; the matrix $[k_3]$ is the sum of five terms. According to the Eq. (32), the fourth term is asymmetric. For convenience, the asymmetric term is separated from the other symmetric ones. At section I, the sum of the symmetric terms is shown. The matrix $[k_3]$ can be expressed in terms of the symmetric and asymmetric parts.

$$[K_0]=\begin{bmatrix} \frac{EA}{L} & 0 & 0 & \frac{-EA}{L} & 0 & 0 \\ 0 & \frac{12EI}{L^3} & \frac{6EI}{L^2} & 0 & \frac{-12EI}{L^3} & \frac{6EI}{L^2} \\ 0 & \frac{6EI}{L^2} & \frac{4EI}{L} & 0 & \frac{-6EI}{L^2} & \frac{2EI}{L} \\ -\frac{EA}{L} & 0 & 0 & \frac{EA}{L} & 0 & 0 \\ 0 & \frac{-12EI}{L^3} & \frac{-6EI}{L^2} & 0 & \frac{12EI}{L^3} & \frac{-6EI}{L^2} \\ 0 & \frac{6EI}{L^2} & \frac{2EI}{L} & 0 & \frac{-6EI}{L^2} & \frac{4EI}{L} \end{bmatrix} \tag{59}$$

$$[K_P]=\begin{bmatrix} \frac{P}{L} & 0 & 0 & \frac{-P}{L} & 0 & 0 \\ 0 & \frac{6P}{5L} & \frac{P}{10} & 0 & \frac{-6P}{5L} & \frac{P}{10} \\ 0 & \frac{P}{10} & \frac{2PL}{15} & 0 & \frac{-P}{10} & \frac{-PL}{30} \\ -\frac{P}{L} & 0 & 0 & \frac{P}{L} & 0 & 0 \\ 0 & \frac{-6P}{5L} & \frac{-P}{10} & 0 & \frac{6P}{5L} & \frac{-P}{10} \\ 0 & \frac{P}{10} & \frac{-PL}{30} & 0 & \frac{-P}{10} & \frac{2PL}{15} \end{bmatrix}+$$

$$\frac{I}{A}\begin{bmatrix} 0 & 0 & 0 & 0 & 0 & 0 \\ 0 & \frac{12P}{L^3} & \frac{6P}{L^2} & 0 & \frac{-12P}{L^3} & \frac{6P}{L^2} \\ 0 & \frac{6P}{L^2} & \frac{4P}{L} & 0 & \frac{-6P}{L^2} & \frac{2P}{L} \\ 0 & 0 & 0 & 0 & 0 & 0 \\ 0 & \frac{-12P}{L^3} & \frac{-6P}{L^2} & 0 & \frac{12P}{L^3} & \frac{-6P}{L^2} \\ 0 & \frac{6P}{L^2} & \frac{2P}{L} & 0 & \frac{-6P}{L^2} & \frac{4P}{L} \end{bmatrix}+ \tag{60}$$

$$2\begin{bmatrix} 0 & \frac{-\Delta M}{L^2} & \frac{M_1}{L} & 0 & \frac{\Delta M}{L^2} & \frac{-M_2}{L} \\ 0 & 0 & 0 & 0 & 0 & 0 \\ 0 & 0 & 0 & 0 & 0 & 0 \\ 0 & \frac{\Delta M}{L^2} & \frac{-M_1}{L} & 0 & \frac{-\Delta M}{L^2} & \frac{M_2}{L} \\ 0 & 0 & 0 & 0 & 0 & 0 \\ 0 & 0 & 0 & 0 & 0 & 0 \end{bmatrix}$$

$$[K_1] = EA\begin{bmatrix} \frac{\Delta u}{L^2} & \frac{6\Delta v}{5L^2} - \frac{\theta_1+\theta_2}{10L} & \frac{\Delta v}{10L} - \frac{4\theta_1-\theta_2}{30} & \frac{-\Delta u}{L^2} & \frac{-6\Delta v}{5L^2} + \frac{\theta_1+\theta_2}{10L} & \frac{\Delta v}{10L} - \frac{4\theta_2-\theta_1}{30} \\ 0 & 0 & 0 & 0 & 0 & 0 \\ 0 & 0 & 0 & 0 & 0 & 0 \\ \frac{\Delta u}{L^2} & \frac{6\Delta v}{5L^2} - \frac{\theta_1+\theta_2}{10L} & \frac{\Delta v}{10L} - \frac{4\theta_1-\theta_2}{30} & \frac{-\Delta u}{L^2} & \frac{-6\Delta v}{5L^2} + \frac{\theta_1+\theta_2}{10L} & \frac{\Delta v}{10L} - \frac{4\theta_2-\theta_1}{30} \\ 0 & 0 & 0 & 0 & 0 & 0 \\ 0 & 0 & 0 & 0 & 0 & 0 \end{bmatrix} +$$

$$EI\begin{bmatrix} 0 & \frac{12\Delta v}{L^4} - \frac{6}{L^3}(\theta_1+\theta_2) & \frac{6\Delta v}{L^3} - \frac{4\theta_1+2\theta_2}{L^2} & 0 & \frac{-12\Delta v}{L^4} + \frac{6}{L^3}(\theta_1+\theta_2) & \frac{6\Delta v}{L^3} - \frac{2\theta_1+4\theta_2}{L^2} \\ 0 & 0 & 0 & 0 & 0 & 0 \\ 0 & 0 & 0 & 0 & 0 & 0 \\ 0 & \frac{-12\Delta v}{L^4} + \frac{6}{L^3}(\theta_1+\theta_2) & \frac{-6\Delta v}{L^3} + \frac{4\theta_1+2\theta_2}{L^2} & 0 & \frac{12\Delta v}{L^4} - \frac{6}{L^3}(\theta_1+\theta_2) & \frac{-6\Delta v}{L^3} + \frac{2\theta_1+4\theta_2}{L^2} \\ 0 & 0 & 0 & 0 & 0 & 0 \\ 0 & 0 & 0 & 0 & 0 & 0 \end{bmatrix} + \quad (61)$$

$$2EI\begin{bmatrix} 0 & 0 & 0 & 0 & 0 & 0 \\ 0 & \frac{12}{L^4}\Delta u & \frac{6}{L^3}\Delta u & 0 & \frac{-12}{L^4}\Delta u & \frac{6}{L^3}\Delta u \\ 0 & \frac{6}{L^3}\Delta u & \frac{4}{L^2}\Delta u & 0 & \frac{-6}{L^3}\Delta u & \frac{2}{L^2}\Delta u \\ 0 & 0 & 0 & 0 & 0 & 0 \\ 0 & \frac{-12}{L^4}\Delta u & \frac{-6}{L^3}\Delta u & 0 & \frac{12}{L^4}\Delta u & \frac{-6}{L^3}\Delta u \\ 0 & \frac{6}{L^3}\Delta u & \frac{2}{L^2}\Delta u & 0 & \frac{-6}{L^3}\Delta u & \frac{4}{L^2}\Delta u \end{bmatrix}$$

$$[K_2]=EA\begin{bmatrix} \frac{\Delta u}{L^2} & 0 & 0 & \frac{\Delta u}{L^2} & 0 & 0 \\ \frac{6\Delta v}{5L^2}-\frac{\theta_1+\theta_2}{10L} & 0 & 0 & \frac{6\Delta v}{5L^2}-\frac{\theta_1+\theta_2}{10L} & 0 & 0 \\ \frac{\Delta v}{10L}-\frac{4\theta_1-\theta_2}{30} & 0 & 0 & \frac{\Delta v}{10L}-\frac{4\theta_1-\theta_2}{30} & 0 & 0 \\ \frac{-\Delta u}{L^2} & 0 & 0 & \frac{-\Delta u}{L^2} & 0 & 0 \\ \frac{-6\Delta v}{5L^2}+\frac{\theta_1+\theta_2}{10L} & 0 & 0 & \frac{-6\Delta v}{5L^2}+\frac{\theta_1+\theta_2}{10L} & 0 & 0 \\ \frac{\Delta v}{10L}-\frac{4\theta_2-\theta_1}{30} & 0 & 0 & \frac{\Delta v}{10L}-\frac{4\theta_2-\theta_1}{30} & 0 & 0 \end{bmatrix}+$$

$$EI\begin{bmatrix} 0 & 0 & 0 & 0 & 0 & 0 \\ \frac{12\Delta v}{L^4}-\frac{6}{L^3}(\theta_1+\theta_2) & 0 & 0 & \frac{-12\Delta v}{L^4}+\frac{6}{L^3}(\theta_1+\theta_2) & 0 & 0 \\ \frac{6\Delta v}{L^3}-\frac{4\theta_1+2\theta_2}{L^2} & 0 & 0 & \frac{-6\Delta v}{L^3}+\frac{4\theta_1+2\theta_2}{L^2} & 0 & 0 \\ 0 & 0 & 0 & 0 & 0 & 0 \\ \frac{-12\Delta v}{L^4}+\frac{6}{L^3}(\theta_1+\theta_2) & 0 & 0 & \frac{12\Delta v}{L^4}-\frac{6}{L^3}(\theta_1+\theta_2) & 0 & 0 \\ \frac{6\Delta v}{L^3}-\frac{2\theta_1+4\theta_2}{L^2} & 0 & 0 & \frac{-6\Delta v}{L^3}+\frac{2\theta_1+4\theta_2}{L^2} & 0 & 0 \end{bmatrix}+ \quad (62)$$

$$2EI\begin{bmatrix} 0 & 0 & 0 & 0 & 0 & 0 \\ 0 & \frac{12}{L^4}\Delta u & \frac{6}{L^3}\Delta u & 0 & \frac{-12}{L^4}\Delta u & \frac{6}{L^3}\Delta u \\ 0 & \frac{6}{L^3}\Delta u & \frac{4}{L^2}\Delta u & 0 & \frac{-6}{L^3}\Delta u & \frac{2}{L^2}\Delta u \\ 0 & 0 & 0 & 0 & 0 & 0 \\ 0 & \frac{-12}{L^4}\Delta u & \frac{-6}{L^3}\Delta u & 0 & \frac{12}{L^4}\Delta u & \frac{-6}{L^3}\Delta u \\ 0 & \frac{6}{L^3}\Delta u & \frac{2}{L^2}\Delta u & 0 & \frac{-6}{L^3}\Delta u & \frac{4}{L^2}\Delta u \end{bmatrix}$$

I. Upper triangular entries for the symmetric terms of the matrix [K_3]:

$$K_3(1,1) = -K_3(1,4) = K_3(4,4) = EA\frac{-\Delta u^2}{L^3} \tag{63a}$$

$$K_3(1,2) = -K_3(1,5) = -K_3(2,4) = K_3(4,5) = EA\frac{\Delta u}{10L^3}\left[12\,\Delta v - L(\theta_1+\theta_2)\right] + EI\,\frac{6\Delta u}{L^5}\left[2\Delta v - L(\theta_1+\theta_2)\right] \tag{63b}$$

$$K_3(1,3) = -K_3(3,4) = EA\frac{\Delta u}{30L^2}\left[3\,\Delta v - L(4\theta_1-\theta_2)\right] + EI\,\frac{2\Delta u}{L^4}\left[3\Delta v - L(2\theta_1+\theta_2)\right] \tag{63c}$$

$$K_3(1,6) = EA\frac{\Delta u}{30L^2}\left[3\,\Delta v + L(\theta_1-4\theta_2)\right] + EI\,\frac{2\Delta u}{L^4}\left[3\,\Delta v - L(\theta_1+2\theta_2)\right] \tag{63d}$$

$$K_3(2,2) = -K_3(2,5) = K_3(5,5) = \frac{3EA}{35L^3}\left[24\Delta v^2 - 6\Delta v L(\theta_1+\theta_2) + L^2(\theta_1^2+\theta_2^2)\right] + \frac{12EI}{35L^5}\left[36\Delta v^2 - 15\Delta v L(\theta_1+\theta_2) - L^2(5\theta_1^2 - 4\theta_1\theta_2 + 5\theta_2^2)\right] + \frac{48EI_2}{5L^7}\left[27\Delta v^2 - 27\Delta v L(\theta_1+\theta_2) + L^2(8\theta_1^2 + 11\theta_1\theta_2 + 8\theta_2^2\right] \tag{63e}$$

$$K_3(2,3) = -K_3(3,5) = \frac{EA}{140L^2}\left[36\Delta v^2 - 24\theta_1\Delta v L + L^2(-\theta_1^2 + 2\theta_1\theta_2 + \theta_2^2)\right] + \frac{EI}{35L^4}\left[90\Delta v^2 - \Delta v L(132\theta_1 + 6\theta_2) + L^2(40\theta_1^2 + 31\theta_1\theta_2 - 23\theta_2^2)\right] + \frac{12EI_2}{5L^6}\left[54\Delta v^2 - \Delta v L(64\theta_1 + 44\theta_2) + L^2(21\theta_1^2 + 22\theta_1\theta_2 + 11\theta_2^2\right] \tag{63f}$$

$$K_3(2,6) = \frac{EA}{140L^2}\left[36\Delta v^2 - 24\theta_2\Delta v L + L^2(\theta_1^2 + 2\theta_1\theta_2 - \theta_2^2)\right] + \frac{EI}{35L^4}\left[90\Delta v^2 - \Delta v L(6\theta_1 + 132\theta_2) - L^2(23\theta_1^2 - 31\theta_1\theta_2 - 40\theta_2^2)\right] + \frac{12EI_2}{5L^6}\left[54\Delta v^2 - \Delta v L(44\theta_1 + 64\theta_2) + L^2(11\theta_1^2 + 22\theta_1\theta_2 + 21\theta_2^2\right] \tag{63g}$$

$$K_3(3,3) = \frac{EA}{210L}\left[18\Delta v^2 - 3\Delta v L(\theta_1-\theta_2) + L^2(12\theta_1^2 - 3\theta_1\theta_2 + \theta_2^2)\right] + \frac{2EI}{105L^3}\left[-90\Delta v^2 - \Delta v L(120\theta_1 - 69\theta_2) + L^2(128\theta_1^2 + 32\theta_1\theta_2 - 19\theta_2^2)\right] + \frac{8EI_2}{5L^5}\left[48\Delta v^2 - \Delta v L(63\theta_1 + 33\theta_2) + L^2(22\theta_1^2 + 19\theta_1\theta_2 + 7\theta_2^2\right] \tag{63h}$$

$$K_3(3,6)=\frac{EA}{420}\left[-6\Delta v(\theta_1+\theta_2)-L(3\theta_1^2-4\theta_1\theta_2+\theta_2^2)\right]+$$
$$\frac{EI}{105L^3}\left[72\Delta v^2-93\Delta vL(\theta_1+\theta_2)+L^2(32\theta_1^2+50\theta_1\theta_2+32\theta_2^2)\right]+ \quad (63i)$$
$$\frac{4EI_2}{5L^5}\left[66\Delta v^2-66\Delta vL(\theta_1+\theta_2)+L^2(19\theta_1^2+28\theta_1\theta_2+19\theta_2^2\right]$$

$$K_3(4,6)=EA\frac{\Delta u}{30L^2}\left[-3\Delta v-L(\theta_1-4\theta_2)\right]+EI\frac{2\Delta u}{L^4}\left[-3\Delta v-L(\theta_1+2\theta_2)\right] \quad (63j)$$

$$K_3(5,6)=\frac{-EA}{140L^2}\left[36\Delta v^2-24\theta_2\Delta vL+L^2(\theta_1^2+2\theta_1\theta_2-\theta_2^2)\right]+$$
$$\frac{-EI}{35L^4}\left[90\Delta v^2-\Delta vL(6\theta_1+132\theta_2)-L^2(-23\theta_1^2+31\theta_1\theta_2+40\theta_2^2)\right]+ \quad (63k)$$
$$\frac{-12EI_2}{5L^6}\left[54\Delta v^2-\Delta vL(44\theta_1+64\theta_2)+L^2(11\theta_1^2+22\theta_1\theta_2+21\theta_2^2\right]$$

$$K_3(6,6)=\frac{EA}{210L}\left[18\Delta v^2-3\Delta vL(\theta_1-\theta_2)+L^2(\theta_1^2-3\theta_1\theta_2+12\theta_2^2)\right]+$$
$$\frac{-2EI}{105L^3}\left[90\Delta v^2-\Delta vL(69\theta_1-120\theta_2)+L^2(19\theta_1^2-32\theta_1\theta_2-128\theta_2^2)\right]+ \quad (63l)$$
$$\frac{8EI_2}{5L^5}\left[48\Delta v^2-\Delta vL(33\theta_1+63\theta_2)+L^2(7\theta_1^2+19\theta_1\theta_2+22\theta_2^2\right]$$

Π. Nonzero entries for the asymmetric term of the matrix [K_3]:

$$K_3(1,2)=-K_3(1,5)=-K_3(4,2)=K_3(4,5)=EI\frac{48(\theta_1-\theta_2)}{L^5}\left[-2\Delta v+L(\theta_1+\theta_2)\right] \quad (64a)$$

$$K_3(1,3)=-K_3(4,3)=\frac{8EI}{L^5}\left[6\Delta v^2-12\Delta v\theta_1L+L^2(5\theta_1^2+2\theta_1\theta_2-\theta_2^2)\right] \quad (64b)$$

$$K_3(1,6)=-K_3(4,6)=\frac{-8EI}{L^5}\left[6\Delta v^2-12\Delta v\theta_2L+L^2(-\theta_1^2+2\theta_1\theta_2+5\theta_2^2)\right] \quad (64c)$$

The subsequent parameters are used in these relations:

$$\Delta u=u_2-u_1$$
$$\Delta v=v_2-v_1 \quad (65)$$
$$\Delta M=M_2-M_1$$

APPENDIX B

The transformation matrix [T] for the plane frame has the succeeding shape:

$$[T]=\begin{bmatrix} Cos\phi & Sin\phi & 0 & 0 & 0 & 0 \\ -Sin\phi & Cos\phi & 0 & 0 & 0 & 0 \\ 0 & 0 & 1 & 0 & 0 & 0 \\ 0 & 0 & 0 & Cos\phi & Sin\phi & 0 \\ 0 & 0 & 0 & -Sin\phi & Cos\phi & 0 \\ 0 & 0 & 0 & 0 & 0 & 1 \end{bmatrix} \quad (66)$$

REFERENCES

1. Safaan SA. Nonlinear behavior of structural plane frames, *J Struct Div*, *ASCE* 1966; **89**(4): 557-79.
2. Mondkar DP, Powell GH. Finite element analysis of non-linear static and dynamic response, *Int J Numr Meth Eng* 1977; **11**(3): 499-520.
3. Meek JL, Tan HS. Geometrically nonlinear analysis of space frames by an incremental iterative technique, *Comput Methods Appl Mech Eng* 1984; **47**(3): 261–282.
4. Greco M, Menin RCG, Ferreira IP, Barros FB. Comparison between two geometrical nonlinear methods for truss analyses, *Struct Eng Mech* 2012; **41**(6): 735-50.
5. Torkamani MAM, Sonmez M. Inelastic large deflection modeling of beam columns, *J Struct Eng*, *ASCE* 2001; **127**(8): 876-87.
6. Yang YB, Lin SP, Wang CM. Rigid element approach for deriving the geometric stiffness of curved beams for use in buckling analysis, *J Struct Eng*, *ASCE* 2007; **133**(12): 1762-71.
7. Conner JJ, Logcher RD, Chan SC. Nonlinear analysis of elastic framed structures, *J Struct Div*, *ASCE* 1968; **94**(6): 1525-47.
8. Powell GH. Theory of nonlinear elastic structures, *J Struct Div*, *ASCE* 1969; **95**(12): 2687-2701.
9. Oran C. Tangent stiffness in plane frames, *J Struct Div*, *ASCE* 1973; **99**(6): 973-85.
10. Oran C. Tangent stiffness in space frames, *J Struct Div*, *ASCE* 1973; **99**(6): 987-1001.
11. Yang TY. Matrix displacement solution to elastica problems of beams and frames, *Int. J Solids Struct* 1973; **9**(7): 829-42.
12. Wen RK, Rahimzadeh J. Nonlinear elastic frame analysis by finite element, *J Struct Div*, *ASCE* 1983; **109**(8): 1952-71.
13. Yang YB, McGuire W. Stiffness matrix for geometric nonlinear analysis, *J Struct Eng*, *ASCE* 1986; **112**(4): 853-77.
14. Spillers WR. Geometrical stiffness matrix for space frames, *Comput Struct* 1989; **36**(1): 29-37.
15. Torkamani MAM, Sonmez M, Cao J. Second-Order elastic plane frame analysis using finite element methods, *J Struct Eng*, *ASCE* 1997; **123**(9): 1225-35.

16. Chang JT. Derivation of the higher-order stiffness matrix of a space frame element, *Finite Elem Des* 2004; **41**(1): 15-30.
17. Torkamani MAM, Shieh JH. Higher-order stiffness matrices in nonlinear finite element analysis of plane truss structures, *Eng Struct* 2011; **33**(12): 3516-26.
18. Rezaiee-Pajand M, Naserian R. Using more accurate strain for three-dimensional truss analysis, *Asian J. Civil Eng* 2015; **17**(1): 107-26.
19. Gorgun H, Yilmaz S. Geometrically nonlinear analysis of plane frames with semi-rigid connections accounting for shear deformations, *Int J Struct Eng Mech* 2012; **44**(4): 539-69.
20. Gorgun H. Geometrically nonlinear analysis of plane frames composed of flexibly connected members, *Int. J Struct Eng Mech* 2013; **45**(3): 634-49.
21. Rezaiee-Pajand M, Kazemian MS, Aftabi S. Static damage identification of 3D and 2D frames, *Mech Based Des Struct Mach* 2014; **42**: 70-96.
22. Rezaiee-Pajand M, Shahabian F, Bambaeechee M. Stability of semi-rigid portal frames with tapered columns and lateral support, *Asian J Civil Eng* 2015; **16**(2):135-59.
23. Rezaiee-Pajand M, Shahabian F, Bambaeechee M. Buckling analysis of semi-rigid gabled frames, *Int J Struct Eng Mech* 2015; **55**(3):605-38.
24. Rezaiee-Pajand M, Gharaei-Moghaddam N. Analysis of 3D Timoshenko frames having geometrical and material nonlinearities, *Int J Mech Sci* 2015; **94-95**: 140-55.
25. Yang YB, Kuo SR. *Theory & Analysis of Nonlinear Framed Structures*, Singapore, 1994.
26. Zienkiewicz OC, Taylor RL. The finite element method for solid and structural mechanics, Butterworth-Heinemann 2005.
27. Chajes A, Churchill JE. Nonlinear frame analysis by finite element methods, *J Struct Eng, ASCE*, 1987; **113**(6): 1221-35.
28. Torkamani MAM, Sonmez M. Solution techniques for nonlinear equilibrium equations Structures Congress, *18th Conference of the Analysis and Computation Specialty, ASCE* 2008; pp.1-17.
29. Rezaee-Pajand M, Ghalishooyan M, Salehi A. Comprehensive evaluation of structural geometrical nonlinear solution techniques Part I: Formulation and characteristics of the methods, *Int J Struct Eng Mech* 2013; **48**(6): 849-78.
30. Crifield MA. A faster modified newton raphson iteration, *Comput Meth Appl Mech Eng* 1979; **20**(3): 267-78.
31. Zinkiewicz OC. Incremental displacement in non-Linear analysis, *Int J Numr Meth Eng* 1971; **3**(4): 587-92.
32. Wempner GA. Discrete approximation related to nonlinear theories of solids, *Int J Solids Struct* 1971; **7**(11): 1581-99.
33. Riks E. The application of Newton's method to the problem of elastic stability, *J Appl Mech* 1972; **39**: 1060-5.
34. Riks E. An incremental approach to the solution of snapping and buckling problems, *Int J Solids Struct* 1979; **15**(7): 529-51.
35. Ramm E. Strategies for tracing the nonlinear response near limit points, *Nonline Finite Elem Anal Struct Mech* 1981; Springer-Verlag Berlin Heidelberg, 63-89.
36. Crisfield MA. A fast incremental/iterative solution procedure that handles snap-through, *Comput Struct* 1981; **13**(1-3): 55-62.

37. Bergan PG. Solution algorithms for nonlinear structural problems, *Comput Struct* 1980; **12**: 497-509.
38. Chan SL. Geometric and material non-linear analysis of beam-columns and frames using the minimum residual displacement method, *Int J Numr Meth Eng* 1988; **26**: 2657-69.
39. Rezaiee-Pajand M, Naserian R. Using residual areas for geometrically nonlinear structural analysis, *Int J Ocean Eng* 2015; **105**: 327-35.
40. Saffari H, Mansouri I. Non-linear analysis of structures using two-point method, *Int J Non-Linear Mech* 2011; **46**(6): 834-40.
41. Saffari H, Mansouri I. An efficient nonlinear analysis of 2D frames using a Newton like technique, *Arch Civil Mech Eng* 2012; **12**(4): 485-92.
42. Saffari H, Mirzai NM, Mansouri I. An accelerated incremental algorithm to trace the nonlinear equilibrium path of structures, *J Solids Struct 2012*; **9**(4): 425-42.
43. Saffari H, Mirzai NM, Mansouri I, Bagheripour MH. Efficient Numerical Methods in Second-Order Inelastic analysis of Space Trusses, *J Comput Civil Eng, ASCE* 2013; **27**(2): 129-38.
44. Rezaiee-Pajand M, Vejdani-noghreiyan HR, Naghavi AR. Four new method for structural critical points, *Mech Based Design Struct Mach* 2013; **41**: 399-420.
45. Rezaiee-Pajand M, Salehi-Ahmadabad M, Ghalishooyan M. Structural geometrical nonlinear analysis by displacement increment, *Asian J Civil Eng* 2014; **15**(5): 633-53.
46. Rezaiee-Pajand M, Estiri H. Computing the structural buckling limit load by dynamic relaxation method, *Int J Non-Linear Mech* 2016; **81**: 245-60.
47. Rezaiee-Pajand M, Estiri H. Finding equilibrium paths by minimizing external work in dynamic relaxation method, *Appl Math Model* 2016; **40**: 10300-22.
48. Rezaiee-Pajand M, Estiri H. A comparison of large deflection analysis of bending plates by dynamic relaxation, *Period Polytech Civil Eng* 2016; 1-27.
49. Rezaiee-Pajand M, Estiri H. Mixing dynamic relaxation method with load factor and displacement increments, *Comput Struct* 2016; **168**: 78-91.
50. El-Ghazaly HA, Monforton GR. Analysis of flexible frames by energy search, *Comput Struct* 1989; **32**(1): 75-86.
51. Williams Fw. An approach to the nonlinear behavior of the members of a rigid jointed plane framework with finite deflections, *J Mech Appl Math* 1964; **17**(4): 451-69.
52. Wood RD, Zienkiewicz OC. Geometrically nonlinear finite element analysis of beams, frames, arches and axisymmetric shells, *J Comput Struct* 1977; **7**(6): 725-735.
53. Rezaiee- Pajand M, Alamatian J. The dynamic relaxation method using new formulation for fictitious mass and damping, *J Struct Eng Mech* 2010; **34**(1): 109-33.
54. Rezaiee-Pajand M, Alamatian J. Automatic DR structural analysis of snap through and snap back using optimized load increments, *J Struct Eng* 2011; **137**(1): 109-16.
55. Rezaee-Pajand M, kadkhodayan M, Alamatian J, Zhang LC. A new method of fictitious viscous damping determination for the dynamic relaxation method, *Comput Struct* 2011; **89**(9-10): 783-94.
56. Rezaee-Pajand M, Ghalishooyan M, Salehi A. Comprehensive evaluation of structural geometrical nonlinear solution techniques Part Π: Comparison efficiencies of the methods, *J Struct Eng Mech* 2013; **48**(6): 879-914.

57. Rezaiee- Pajand M, Alamatian J. Implicit higher order accuracy method for numerical integration in dynamic analysis, *J Struct Eng* 2008; **134**(6): 973-85.
58. Rezaiee-Pajand M, Sarafrazi SR, Rezaiee H. Efficiency of dynamic relaxation methods in nonlinear analysis of truss and frame structures, *Comput Struct* 2012; **112-113**: 295-310.
59. Rezaiee-Pajand M, Afsharimoghadam H. Optimization formulation for nonlinear structural analysis, *Int J Optim Civil Eng* 2017; **7**(1): 109-27.